Transmission distortion and genetic incompatibilities between alleles in a multigenerational mouse advanced intercross line

Danny Arends, danny.arends@hu-berlin.de, Albrecht Daniel Thaer-Institut für Agrar- und Gartenbauwissenschaften, Humboldt-Universität zu Berlin, Invalidenstraße 42, D-10115 Berlin, Germany

Stefan Kärst, stefan.kaerst@outlook.com, Albrecht Daniel Thaer-Institut für Agrar- und Gartenbauwissenschaften, Humboldt-Universität zu Berlin, Invalidenstraße 42, D-10115 Berlin, Germany

Sebastian Heise, SebastianHeise81@gmx.de, Albrecht Daniel Thaer-Institut für Agrar- und Gartenbauwissenschaften, Humboldt-Universität zu Berlin, Invalidenstraße 42, D-10115 Berlin, Germany

Paula Korkuc, paula.korkuc@hu-berlin.de, Albrecht Daniel Thaer-Institut für Agrar- und Gartenbauwissenschaften, Humboldt-Universität zu Berlin, Invalidenstraße 42, D-10115 Berlin, Germany

Deike Hesse, deike.hesse-wilting@hu-berlin.de, Albrecht Daniel Thaer-Institut für Agrar- und Gartenbauwissenschaften, Humboldt-Universität zu Berlin, Invalidenstraße 42, D-10115 Berlin, Germany

Gudrun A. Brockmann[†], gudrun.brockmann@hu-berlin.de, Albrecht Daniel Thaer-Institut für Agrar- und Gartenbauwissenschaften, Humboldt-Universität zu Berlin, Invalidenstraße 42, D-10115 Berlin, Germany

[†] To whom correspondence should be addressed.

Address for correspondence

Gudrun A. Brockmann

Phone: 0049 30 2093 6089

Fax: 0049 30 2093 6397

E-mail: gudrun.brockmann@agrar.hu-berlin.de

Running title: TRD in mouse advanced intercross line

Keywords: Intergenerational effects, Non-Mendelian inheritance, Genetic incompatibilities, Interactions, Allele Transmission Bias

Abstract

Background/Objectives

While direct additive and dominance effects on complex traits have been mapped repeatedly, additional genetic factors contributing to the heterogeneity of complex traits have been scarcely investigated. To assess genetic background effects, we investigated transmission ratio distortions (TRDs) of alleles from parent to offspring using an advanced intercross line (AIL) of an initial cross between the mouse inbred strains C57BL/6NCrl (B6N) and BFMI860-12 (BFMI).

Subjects/Methods

341 males of generation 28 and their respective 61 parents and 66 grandparents were genotyped using Mega Mouse Universal Genotyping Arrays (MegaMUGA). TRDs were investigated using allele transmission asymmetry tests, and pathway overrepresentation analysis was performed. Sequencing data was used to test for overrepresentation of non-synonymous SNPs in TRD regions. Genetic incompatibilities were tested using the Bateson-Dobzhansky-Muller two-locus model.

Results

62 TRD regions were detected, many in close proximity to the telocentric centromere. TRD regions contained 44.5% more non-synonymous SNPs than randomly selected regions (182 vs. 125.9 ± 17.0, $P < 1x10^{-4}$). Testing for genetic incompatibilities between TRD regions identified 29 genome-wide significant incompatibilities between TRD regions ($P_{(BF)} < 0.05$). Pathway overrepresentation analysis of genes in TRD regions showed that DNA methylation, epigenetic regulation of RNA, and meiotic/meiosis regulation pathways were affected independent of the parental origin of the TRD. Paternal BFMI TRD regions showed overrepresentation in the small interfering RNA (siRNA) biogenesis and in the metabolism of lipids and lipoproteins. Maternal B6N TRD regions harbored genes involved in meiotic recombination, cell death, and apoptosis pathways. The analysis of genes in TRD regions suggests the potential distortion of protein-protein interactions influencing obesity and diabetic retinopathy as a result of disadvantageous combinations of allelic variants in *Aass*, *Pgx6* and *Nme8*.

Conclusions

56 Using an AIL significantly improves the resolution at which we can investigate TRD. Our analysis
57 implicates distortion of protein-protein interactions as well as meiotic drive as the underlying
58 mechanisms leading to the observed TRD in our AIL. Furthermore, genes with large amounts of non-
59 synonymous SNPs located in TRD regions are more likely to be involved in pathways that are related
60 to the phenotypic differences between the parental strains. Genes in these TRD regions provide new
61 targets for investigating genetic adaptation, protein-protein interactions, and determinants of complex
62 traits such as obesity.

63 *Introduction*

64 Over the last two decades genome wide association studies (GWAS) have identified a virtual avalanche
65 of genetic variants associated with complex phenotypes and diseases (Buniello et al. 2019). However,
66 although numerous, these identified genetic variations only partially explain the observed heritability
67 in complex phenotypes either individually or combined (Zuk et al. 2012). This so called "missing
68 heritability" problem has been observed for many complex phenotypes and diseases, such as obesity
69 which has long been known to be a major risk factor for many diseases in the later course of life
70 (Kopelman 2007; Tremmel et al. 2017). For obesity, as well as other complex phenotypes, a great
71 amount of effort was spent finding genetic determinants (Speliotes et al. 2010; Willer et al. 2009). As
72 a result, a large number of genetic variants contributing to obesity have been identified
73 (www.genome.gov/gwastudies). However, most loci found by GWAS had small effects (Willer et al.
74 2009; Shungin et al. 2015). For example, the 97 significant loci identified for body mass index (BMI),
75 accounted for only 2.7% of the corresponding variation (Locke et al. 2015).

76 One of several reasons discussed for the "missing heritability" problem in GWAS is the genetic
77 heterogeneity of loci contributing to complex traits among the individuals in populations (Shungin et
78 al. 2015; Heid et al. 2010). In addition to direct genetic effects, substantial phenotypic variation among
79 individuals can be caused by preferential allele combinations or by allele incompatibilities in the
80 genome of individuals. Allele incompatibilities are combinations of two (or more) alleles which when

81 inherited together cause a disadvantage for the individual. Inheriting the disadvantageous allele
82 combination leads to a survival disadvantage for this individual (e.g. less vigor, less successful
83 reproduction). Allelic interactions leading to such disadvantages can be detected as transmission ratio
84 distortion (TRD) from parent to offspring (also called allele transmission bias). Although TRD has been
85 widely reported in a wide range of species (Huang et al. 2013b; Lyon 2003; Li et al. 2019), its functional
86 impact on complex phenotypes has rarely been studied.

87 To investigate genetic background effects such as TRD, we examined three generations (26, 27, and
88 28) of an advanced intercross line (AIL) between two inbred mouse lines, the Berlin Fat Mouse Inbred
89 (BFMI) line and C57BL/6NCrl (B6N) line. In AIL populations from two inbred founders, only two parental
90 alleles can segregate at each locus, making the population heterogeneous but less complex than
91 human populations. Therefore, an AIL population is well suited to study deviations from Mendelian
92 inheritance.

93 The BFMI is an inbred line generated from an outbred population descending from several different
94 founder mice bought at pet shops across Berlin. The BFMI line had been selected for high fatness for
95 more than 100 generations before it was inbred (Wagener et al. 2006). Unfortunately, the original
96 founders of the BFMI do not exist anymore. However, whole genome DNA sequencing data showed
97 that the BFMI genome is a mixture of *Mus musculus musculus* and *Mus musculus domesticus*.

98 Recently, a major recessive mutation responsible for the juvenile obesity phenotype (*jObes1*) in BFMI
99 mice was fine-mapped to a 370 kb region on chromosome 3 (Arends et al. 2016). Complementation
100 tests suggested *Bbs7* as the most likely causal gene in this region. The *jObes1* locus accounted for
101 around 40% of the body weight variance (Neuschl et al. 2010; Arends et al. 2016), while environmental
102 effects accounted for 34%. Hence, around 26% of the variance in body weight is still unexplained.

103 During the process of long-term selection for a phenotype (e.g. high fatness), enrichment or even
104 fixation of alleles that positively contributed to the selection response have been observed (Hirsch et
105 al. 2014). Complimentary, the frequency of conflicting alleles impairing fitness, survival of gametes or

106 embryos would be expected to be reduced or lost in the process of selection. In particular in complex
107 traits, such as obesity, where many genes with diverse allelic variants contribute to the phenotype, the
108 compatibility of interacting alleles is expected to be a driving force for the selection response.
109 Therefore, long-term selection can be considered as co-evolution of alleles during the process of
110 adaptation to selection pressure, environment, and genetic background.

111 The same principles of shaping the genomic composition occurred during the inbreeding history of
112 every inbred mouse line, including BFMI and B6N, which were used in our experiment. Experimental
113 inbreeding usually starts with several full-sib families (Flurkey et al. 2009). During the process of
114 repeated mating of full-sibs, when the genome gets more and more reduced to one haplotype, some
115 inbred families go extinct because of direct lethal recessive allele effects, lethal combinations of alleles
116 across the genome, or the inbred family collapses because of low vigor or insufficient reproduction
117 (Whitlock 2000; Fitzpatrick and Evans 2009; Zajitschek et al. 2009) eventually as a result of genomic
118 incompatibility. However, low level incompatibilities, which do not directly cause lethality or affect
119 fertility might be retained, invisible, inside an inbred line. During the inbreeding process haplotypes
120 get reduced, and incompatibilities might survive since there is no choice of alternative allele anymore.
121 In the end, a kind of optimized genome remains alive as established inbred strain.

122 ## Results

123 ### *Allele transmission ratios from heterozygous parents to offspring*

124 The probability for the transmission of parental alleles to their offspring can be calculated according
125 to Mendelian laws. Deviations from those expected inheritance patterns might have genetic reasons
126 that we intend to identify. To test for TRDs, we used all 341 males of generation 28 of the AIL and
127 tested how their parents (generation 27) transmitted their alleles to this generation. TRD was detected
128 for 62 genomic regions at a genome-wide Bonferroni corrected significance level of 0.01. These regions
129 can be grouped by the preferentially transmitted allele based on the parental origin (paternal /
130 maternal) and the founder strain origin (B6N / BFMI). Significant paternal allele TRD was detected for
131 1,068 out of 18,114 tested SNPs. Paternally affected TRD of SNPs clustered into 31 chromosomal
132 regions, due to linkage between neighboring SNPs. For maternal TRD, 1,138 SNPs located in 31 regions
133 were found (Supplemental_Table_S1). Overlaying the paternal and maternal TRD regions showed that
134 14 regions showed both paternal and maternal TRD. In overlapping TRD regions always the same
135 founder allele of either mouse strain B6N or BFMI was preferentially transmitted.

136 TRD was detected consistently across large genomic regions, in which a high number of markers
137 showed the same transmission bias for one of the two founder alleles B6N or BFMI. The 19 regions
138 showing TRD supported by at least 50 markers are shown in Table 1, all detected TRD regions and their
139 observed transmission distortions are summarized in Supplemental_Table_S1, and visualized in Figure
140 1. Genotypes, genetic map, and pedigree of the AIL individuals can be found in
141 Supplemental_Table_S2.

142 As an example, Pat_R3 is a region on chromosome 4 from 3.5 to 12.5 Mb, which showed paternal TRD
143 of the BFMI allele supported by 83 markers. In the AIL population, we observed at each marker around
144 217 paternal allele transmissions from generation 27 to 28, meaning we expect 108.5 transmissions of
145 the BFMI, as well as 108.5 transmissions of the B6N allele. However, in this region markers on average
146 showed 168 (+/- 5.0) transmissions of the BFMI allele from heterozygous fathers to their offspring,

147 while the B6N allele was only transmitted 55.3 (+/- 3.9) times. At the top marker in this region on
148 chromosome 4 (UNC6664886), we observed 169 BFMI versus 48 B6N transmissions. This means that
149 transmission of the BFMI allele was observed 55.8 % more often than expected by Mendelian
150 inheritance, the likelihood of this happening was estimated by χ^2-test to be lower than $1x10^{-14}$.

151 When performing the same tests for the allele transmission from AIL generation 26 to 27 (transmission
152 from grandparents (n = 66) to parents (n = 61)), where sample sizes were much smaller, we relaxed
153 our threshold for significance to $p < 0.05$. In generation 26 to 27, 0 and 38 SNPs still showed significant
154 paternal or maternal TRD, respectively. The overlap between SNPs detected in generations 26 to 27
155 versus 27 to 28 was 100%, meaning that all TRD seen from generation 26 to 27 was also found (much
156 more significant) from generations 27 to 28.

157 ***Table 1: Transmission ratio distortion from paternal and maternal side, supported by at least 50 SNPs (p < 0.01) per identified region.*** *Region ID = the identifier of the region Pat_R# stands for*
158 *paternal transmission ratio distortion and Mat_R# stands for maternal transmission ratio distortion within the region, Chr = Chromosome on which the distortion was detected. Proximal, Top, and*
159 *Distal = start, top, and end positions of the region on the chromosome (based on the GRCm38.p6 / mm10 genome), preferred allele = the allele preferentially transmitted, nSNPs = number of SNP*
160 *markers on the array that support the TRD region, average transmission counts for founder alleles across all markers in the region are listed with their standard deviation in brackets. Top marker*
161 *as well as transmission at the top marker and BFMI allele % distortion is shown in the last 4 columns. See Supplemental_Table_S1 for an overview of all 31 paternal and 31 maternal regions. The*
162 *observed very small standard deviations in almost all regions indicate that the distortion observed is consistent across the regions identified.*

RegionID	Chr	Proximal	Top	Distal	RegionSize	nSNPs	Prefered Allele	Transmissions regionaverage (SD)		Topmarker	Transmission Topmarker		BFMIallele %distortion
								BFMI	B6N		BFMI	B6N	
Pat_R1	1	3,668,628	11,643,615	14,698,538	11,029,910	68	BFMI	146.1 (16.3)	41.1 (6.6)	UNC109624	152	30	67.0
Pat_R3	4	3,569,913	6,093,982	12,555,306	8,985,393	83	BFMI	168.0 (5.0)	55.3 (3.9)	UNC6664886	169	48	55.8
Pat_R7	4	76,193,199	78,074,351	81,245,565	5,052,366	58	BFMI	79.6 (9.0)	15.8 (3.0)	UNC7556251	84	15	69.7
Pat_R17	12	5,253,913	8,416,509	12,177,986	6,924,073	92	BFMI	163.3 (28)	53.5 (9.6)	UNC20594325	207	47	63.0
Pat_R21	16	5,617,528	14,151,479	14,151,479	8,533,951	93	B6N	31.5 (7.2)	147.9 (15.1)	UNC26373573	35	177	-67.0
Pat_R22	17	3,264,958	5,991,544	11,318,508	8,053,550	77	B6N	34.0 (16.2)	99.4 (27.1)	UNC170286629	16	139	-79.4
Pat_R23	17	47,490,686	48,644,966	50,134,302	2,643,616	50	B6N	41.7 (30.8)	117.1 (10.1)	UNC27963988	19	110	-70.5
Pat_R24	18	4,516,519	12,242,865	13,902,153	9,385,634	71	BFMI	158.7 (2.9)	61.4 (3.3)	UNC28742422	155	56	46.9
Pat_R25	18	38,281,545	38,975,190	42,987,483	4,705,938	54	BFMI	168.7 (4.1)	54.2 (9.3)	UNC29080241	168	46	57.0
Mat_R1	1	3,668,628	3,668,628	21,099,704	17,431,076	94	BFMI	136.2 (17.8)	56.9 (10.3)	UNC010515443	178	69	44.1
Mat_R2	3	6,274,425	11,119,314	17,230,305	10,955,880	53	B6N	24.9 (13.5)	129.2 (5.8)	backupUNC030002827	13	126	-81.3
Mat_R5	3	133,540,430	136,529,917	137,921,098	4,380,668	52	B6N	35.4 (4.1)	105.3 (12.8)	UNC6326383	33	113	-54.8
Mat_R6	4	3,569,913	3,918,966	12,555,306	8,985,393	83	BFMI	144.5 (5.5)	50.1 (6.4)	UNC6640040	135	38	56.1
Mat_R12	6	48,276,599	48,276,599	53,750,577	5,473,978	53	B6N	24.8 (5.0)	80.5 (15.4)	UNC11030573	27	96	-56.1
Mat_R15	9	67,022,716	74,576,994	75,773,843	8,751,127	54	B6N	37.3 (12.9)	110.8 (16.1)	UNC090145124	23	99	-62.3
Mat_R16	9	106,017,492	106,605,721	107,516,430	1,498,938	58	B6N	29.3 (4.5)	87.1 (2.4)	UNC17077906	27	87	-52.6
Mat_R23	16	5,617,528	5,617,528	18,450,764	12,833,236	163	B6N	23.5 (8.7)	108.4 (11.2)	UNC160000883	10	130	-85.7
Mat_R25	17	3,264,958	5,991,544	11,318,508	8,053,550	77	B6N	20.0 (4.4)	106.8 (22.4)	UNC170286629	20	164	-78.3
Mat_R28	18	4,516,519	8,317,246	15,000,978	10,484,459	81	BFMI	170.6 (19.5)	52.0 (2.8)	UNC28690832	50	197	-59.5

163

164 In our population, we observed that the TRD is a local event affecting many SNPs in a well-defined
165 chromosomal region due to linkage between neighboring SNPs. Since, many recombinations have
166 accumulated over 28 generations of mating, the length of the TRD affected regions is between 41.1 kb
167 and 17.4 Mb (Supplemental_Table_1). In these regions, SNPs that showed TRD are tightly linked
168 (Figure 1), which can be seen by TRD SNPs clustering together into regions. Very small standard
169 deviations of averaged TRD transmissions (Table 1) were observed for all regions, which indicates that
170 distortion observed was consistent across the TRD region. This was further supported by the
171 observation that all SNPs in a certain region always showed the same direction of transmission towards
172 one of the alleles from the original founder strains of the AIL population. For example, Mat_R1 showed
173 the BFMI allele was preferentially transmitted in the maternally distorted region on chromosome 1
174 between 3.7 and 21.1 Mb. For the 94 markers in this region, we observed 136.2 +/- 17.8 transmissions
175 of the BFMI allele versus 56.9 +/- 10.3 transmissions of the B6N allele from mother generation 27 to
176 offspring (generation 28).

177 Interestingly, regions showing significant TRD on 10 out of 19 autosomes (autosomes 1, 3, 4, 5, 10, 12,
178 14, 16, 17, 18) are located close to the telocentric centromere (Figure 1). These 10 telocentric
179 centromere regions showed both paternal and maternal TRD with a consistent preference of the
180 founder allele. While these telocentric centromere regions showed TRD for both paternal and maternal
181 alleles, we observed that non-telocentric centromere regions (e.g. Mat_R12, Table 1) tend to show
182 TRD only when inherited from either the paternal or the maternal side.

183 ***Genetic variants in TRD regions***

184 To identify candidate genes for each region, and to investigate possible causes for the observed TRD,
185 protein coding genes located in TRD regions were examined. Sequence variants were detected by
186 comparing the BFMI sequence to the B6N reference genome (ENSEMBL, GRCm38.p6)
187 (Supplemental_Table_S3). In the 62 identified TRD regions, 1,167 unique protein coding genes were
188 located. In detail, these were 292 genes in Pat_BFMI regions, 362 in Mat_BFMI, 335 in Pat_B6N, and
189 567 in Mat_B6N. Among those, 389 genes were overlapping between paternal and maternal TRD
190 regions.

191 In the 1,167 unique protein coding genes located in 62 TRD regions, 182 non-synonymous SNPs
192 (nsSNPs) were found located in 128 (10.9%) genes. Permutation analysis showed that the density of
193 nsSNPs in the TRD regions was 1.445 times higher than expected from random distribution. Results
194 from 50,000 permutations showed an average of 125.9 ± 17.0 (SD) nsSNPs per 1,167 randomly selected
195 genes with a maximum value of 180 SNPs observed during permutation. These results provide
196 evidence that nsSNPs are significantly overrepresented in TRD regions ($P < 1x10^{-4}$).

197 ***Figure 1: Genomic regions showing allele transmission ratio distortion towards generation 28.*** *Bars left of the*
198 *chromosomes mark the SNPs which show paternal TRD (♂); bars on the right side show maternal TRD (♀), using a genome*
199 *wide significance level of P < 0.01. Colors show the origin of the allele preferentially transmitted, blue: B6N allele, orange:*
200 *BFMI allele. Chromosomal black areas (suitable markers) contain markers which passed quality control steps, segregate*
201 *between the founder lines (BFMI and B6N), and have at least ten heterozygous parents in generation 27 required to perform*
202 *a valid X^2 test. Chromosomal beige areas (Founders equal) are markers at which the BFMI and B6N have the same allele,*
203 *these markers do not segregate in the AIL population, and cannot be tested for TRD. Chromosomal gray areas (unsuitable*
204 *markers) have not been tested due to lack of heterozygous parents in generation 27 at these markers. Chromosomal red*
205 *areas are not in Hardy-Weinberg equilibrium (HWE) in generation 28, since HWE is an assumption underlying a valid TRD*
206 *test, these areas were excluded from TRD analysis.*

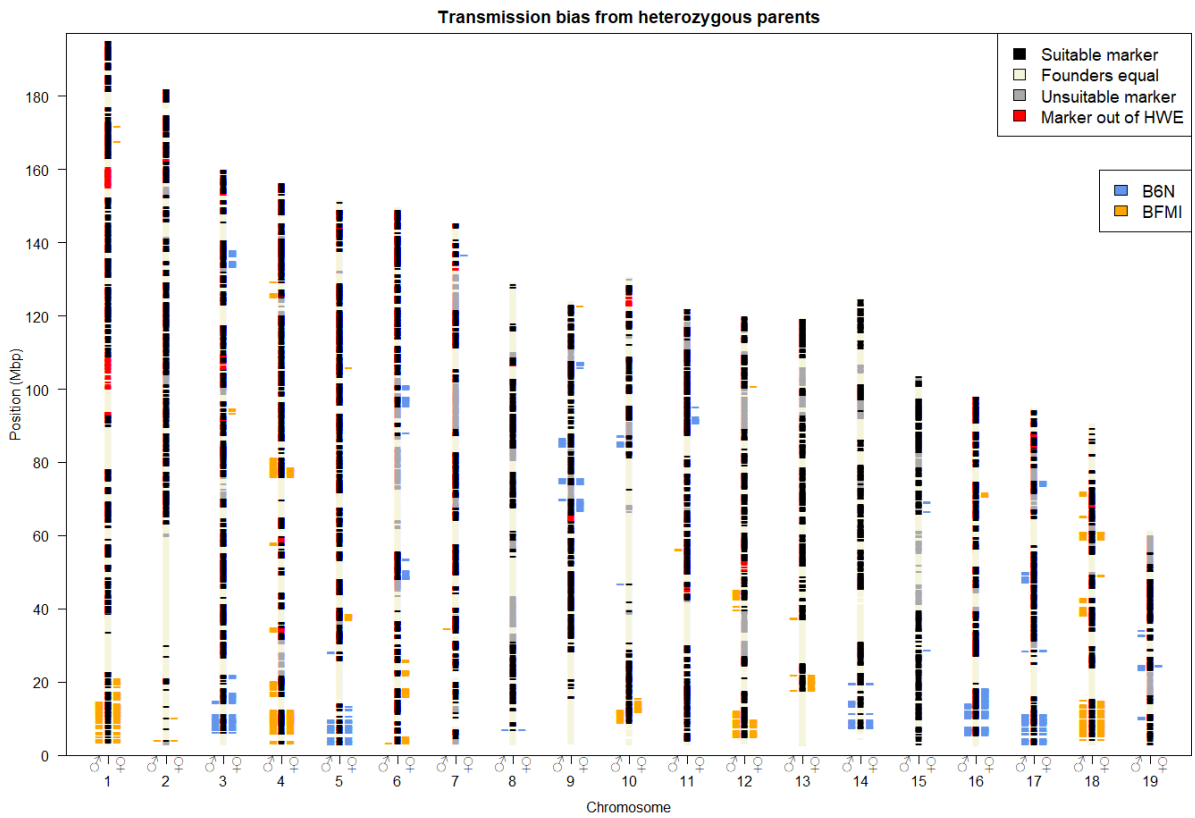

207

208 *Pathway overrepresentation analysis*

209 Pathways analysis was performed twice, once we investigated pathway overrepresentation by
210 including all protein-coding genes in the specified TRD regions, followed by only investigating genes
211 that carry nsSNPs.

212 Analysis of all genes in TRD regions with higher transmission of the paternal BFMI allele (Pat_BFMI)
213 showed slight but significant pathway overrepresentation of the three pathways "Post-transcriptional
214 silencing by small RNAs" ($P_{(BH)} = 0.008$), "Small interfering RNA (siRNA) biogenesis" ($P_{(BH)} = 0.011$), and
215 "MicroRNA (miRNA) biogenesis" ($P_{(BH)} = 0.016$) (Supplemental_Table_S4 - Pat_BFMI for the full list).

216 All genes located in maternal inherited (Mat_BFMI) showed highly significant overrepresentation for
217 pathways such as "DNA methylation" ($P_{(BH)} < 5.7x10^{-16}$), "Meiotic Recombination" ($P_{(BH)} < 6.61x10^{-15}$),
218 "Packaging Of Telomere Ends" ($P_{(BH)} < 1.70x10^{-13}$), "Chromatin organization" ($P_{(BH)} < 2.66x10^{-10}$) and
219 "Deposition of new CENPA-containing nucleosomes at the centromere" ($P_{(BH)} < 3.67x10^{-10}$)
220 (Supplemental_Table_S4 - Mat_BFMI for the full list). All these pathways are involved in chromosome
221 stability/maintenance as well as centromere and nucleosome organization. We also found strong
222 overrepresentation of the "Signaling by Wnt" ($P_{(BH)} = 1.09x10^{-5}$) pathway, as well a weak
223 overrepresentation of the "Retinol metabolism" ($P_{(BH)} = 0.010$) pathway. These are two interesting
224 pathways in the context of BFMI mice, which will be elaborated in more detail in the discussion section.

225 No strong overrepresentation or overlap was found for all genes located in paternal/maternal B6N TRD
226 regions (Supplemental_Table_S4 - Pat_B6N & Mat_B6N). Only three pathways were found weakly
227 overrepresented when using all genes from maternal B6N (Mat_B6N) TRD regions: "Nitrogen
228 metabolism" ($P_{(BH)} < 0.019$), "Reversible hydration of carbon dioxide" ($P_{(BH)} < 0.033$), and "Osteoclast
229 differentiation" ($P_{(BH)} < 0.042$).

230 If we focused on genes with nsSNPs in TRD regions, where the BFMI allele is preferentially passed by
231 the father (Supplemental_Table_S4 - Pat_BFMI_SNP), no strong pathway overrepresentation was
232 observed. Only two pathways reach significance after Benjamini-Hochberg correction: "S Phase" ($P_{(BH)}$

233 = 0.015) and “Extracellular matrix organization” ($P_{(BH)}$ = 0.025). However, the number of genes found
234 in TRD regions (2 for both) versus the total number of genes annotated to these pathways make this
235 overrepresentation very weak (117 and 216 respectively). If we examined the genes with nsSNPs from
236 TRD regions of paternal B6N allele transmission (Supplemental_Table_S4 - Pat_B6N_SNP), “Interferon
237 Signaling” ($P_{(BH)}$ = 0.016), “Cell cycle” ($P_{(BH)}$ = 0.023), and “Metabolism of lipids and lipoproteins” ($P_{(BH)}$
238 = 0.023) were weakly significantly overrepresented. Again, the numbers of genes in TRD regions is
239 small compared to the total number of genes annotated to these pathways.

240 Genes with nsSNPs from TRD regions of the maternal BFMI allele (Supplemental_Table_S4 -
241 MAT_BFMI_SNP) showed only one very weak significant pathway overrepresentation: “Extracellular
242 matrix organization” ($P_{(BH)}$ = 0.046), which was also found for genes with nsSNPs in TRD regions where
243 the BFMI allele was preferentially passed by the father (Pat_BFMI_SNP). Genes with nsSNPs in TRD
244 regions of the maternal B6N allele (Supplemental_Table_S4 - Mat_B6N_SNP) also showed
245 overrepresentation of multiple pathways overlapping with pathways found for genes with nsSNPs in
246 paternal B6N regions (“Cell cycle”, “Interferon Signaling”, “Metabolism”, and “Metabolism of lipids and
247 lipoproteins”). Furthermore, maternal genes with nsSNPs in TRD regions contributed also to cell death
248 and apoptosis (pathways “Cell death signalling via NRAGE, NRIF and NADE” ($P_{(BH)}$ = 0.04) and “p75 NTR
249 receptor-mediated signaling” ($P_{(BH)}$ = 0.049)).

250 ***Genetic incompatibilities***

251 Since functional inaptitude of alleles of interacting pairs of genes could be causal for TRD, we searched
252 for evidence of genetic incompatibilities by a pairwise search between all 62 TRD regions against each
253 other using the Bateson-Dobzhansky-Muller model. This test identifies outliers (significant deviation
254 from Mendelian expectation) between allele pairs by investigating allele frequencies. Severe
255 deviations from Mendelian expectation is interpreted as resulting from negative epistatic interactions
256 between incompatible loci. This search identified genome-wide significant pairwise incompatibilities
257 ($P_{(BF)} < 0.05$) for 29 out of 62 TRD regions (Figure 2), of which 19 were classified as highly significant
258 ($P_{(BF)} < 0.01$). The high number of TRD regions (46.8 %) showing evidence for one or more genetic
259 incompatibilities suggests that genetic incompatibilities are an important contributor to TRD.

260 Analysis of protein-protein interactions between all 128 protein-coding genes with nsSNPs located in
261 TRD regions showed 331 known interactions between the protein products of these genes. When we
262 ignored genes located on the same chromosome (for which genetic incompatibility tests cannot be
263 performed) we ended up with 273 known protein-protein interactions.

264 Within the 29 regions that showed genome-wide evidence ($P_{(BF)} < 0.05$) for genetic incompatibilities,
265 44 out of the 128 (34.4%) protein-coding genes with nsSNPs reside. In total, five known physical
266 protein-protein interactions exist in the Search Tool for the Retrieval of Interacting Genes/Proteins
267 (STRING) database between these 44 genes.

268 Within these known protein-protein interactions, we found an interaction between alpha-aminoadipic
269 semialdehyde synthase (Aass) located in Mat_R11 (6:16-26 M) with glutathione peroxidase 6 (Pgx6) as
270 well as NME/NM23 Family Member 8 (Nme8) which are both located in Mat_R20 (13:18-22 M). All
271 three of these genes are interesting, given that all three genes are involved in obesity and/or diabetic
272 retinopathy, which are the obvious phenotypic difference between the founders inbred strains BFMI
273 and B6N. The Aass protein is involved in the major mitochondrial lysine degradation pathway (Papes
274 et al. 1999; Sacksteder et al. 2000) and was found to be downregulated in obese compared with lean

275 co-twins (Heinonen et al. 2015). With regard to Pgx6, glutathione peroxidase activity is suppressed in
276 diabetic compared to healthy controls, with a more pronounce suppression in obese compared to
277 nonobese diabetics (Singhai et al. 2011). Glutathione peroxidase activity was found associated with
278 diabetic retinopathy (Rodríguez-Carrizalez et al. 2014). Nme8, encodes an axoneme protein, and
279 mutations in the *Nme8* gene have been implicated to cause primary ciliary dyskinesia (Duriez et al.
280 2007). Furthermore, the genetic region in which the *Nme8* gene is located was identified in human
281 GWAS as a locus which might be involved in childhood obesity in the Hispanic population (Comuzzie
282 et al. 2012). *Nme8* is a very interesting gene to come up during this analysis, because of its relation to
283 primary ciliary dyskinesia. The *Bbs7* gene was previously identified as the most likely causal gene for
284 the obesity phenotype of the BFMI mouse (Arends et al. 2016). The Bbs7 protein is part of the BBSome
285 complex which is a heterooctameric protein complex that plays a central role in primary cilia
286 homeostasis (Klink et al. 2020).

287 Furthermore, a protein-protein interaction between acyloxyacyl hydrolase (Aoah), located Mat_R20
288 (13:18-22 M) and protein tyrosine phosphatase receptor type Z1 (*Ptprz1*) Mat_R11 (6:16-26 M) was
289 found. Aoah is a lipase that plays an important role in the defense against gram-negative bacterial
290 infection (Lu et al. 2008). Aoah$^{-/-}$ mice on a high-carbohydrate diet develop non-alcoholic
291 steatohepatitis (NASH) and both serum triglyceride and cholesterol were found significantly increased
292 (Ojogun 2008). The *Ptprz1* gene is annotated to the insulin receptor recycling pathway, and protein
293 tyrosine phosphatases (PTPs) are required for the dephosphorylation of the insulin receptor (Fischer
294 et al. 1991). Again, both genes identified by our approach are clear candidate genes when considering
295 the major phenotypic differences of the founder strains BFMI and B6N.

296 The next identified protein-protein interaction between genes with nsSNPs in TRD regions showing
297 genetic incompatibilities was between myosin IE (Myo1e), located Mat_R15 (9:67-76 M) and
298 serine/threonine kinase 32B (Stk32b) Mat_R9 (5:37-39 M). Myo1e is part of the nonmuscle class I
299 myosins which are a subgroup of the unconventional myosin protein family and function as actin-based
300 molecular motor. The *Stk32b* gene is annotated into the “Sweet Taste Signaling” pathway (GeneCards

301 Human Gene Database 2021), and deletion of the gene was associated with Ellis-Van Creveld
302 Syndrome (Temtamy et al. 2008) in humans. This interaction doesn't have a clear link to the phenotypic
303 differences between BFMI and B6N.

304 Moreover, protein-protein interaction was detected between myosin VC (Myo5c), located Mat_R15
305 (9:67-76 M) and solute carrier family 2 member 9 (Slc2a9) located in Mat_R9 (5:37-39 M). The Myo5c
306 protein is involved in actin-based membrane trafficking in many physiologically crucial tissues. In
307 humans (and mice), Myo5c is particularly abundant in epithelial and glandular tissues such as:
308 pancreas, prostate, mammary, stomach, colon, and lung (Rodriguez and Cheney 2002). *Myo5c*
309 knockout mice show a decrease in total body fat amount and an increased lean body weight (Blake et
310 al. 2021; Mouse Genome Database (MGD) 2021). It's protein interaction partner Glut9 (*Slc2a9*) is part
311 of the SLC2A facilitative glucose transporter family. Members of this family play a role in maintaining
312 glucose homeostasis. Glut9 does not transport glucose, but is classified as a urate transporter.
313 Mutations in the *Slc2a9* gene have been shown to be causal for renal hypouricemia (Matsuo et al.
314 2008; Dinour et al. 2010), mice lacking the Glut9 protein show early onset metabolic syndrome
315 (DeBosch et al. 2014).

316 These known protein-protein interactions between genes in TRD regions with nsSNPs, lead us to
317 hypothesize that disturbed protein-protein interactions resulting from amino acids changes due to
318 nsSNPs within several proteins of a protein complex are likely one of the driving forces causing the TRD
319 observed in the BFMIxB6N advanced intercross line.

Figure 2: Significant genetic incompatibilities between regions showing TRD. *Heat map showing the pairwise genetic incompatibility scan between TRD regions, genome-wide $P_{(BF)} < 0.05$. The allele combination (M1|M2) which is most reduced (in percentages) between the observed and expected allele combinations are shown in the figure with colors denoting the founder allele combination M1 (x-axis) and M2 (y-axis). Names of regions are composed of chr:start-end allele origin; start and end positions are given in megabase pairs; furthermore, the TRD origin is coded by M for maternal and P for paternal. When two regions were located on the same chromosome the genetic incompatibility test was not performed (gray areas), since the pairwise genetic incompatibility test can only be performed on loci which are not in linkage.*

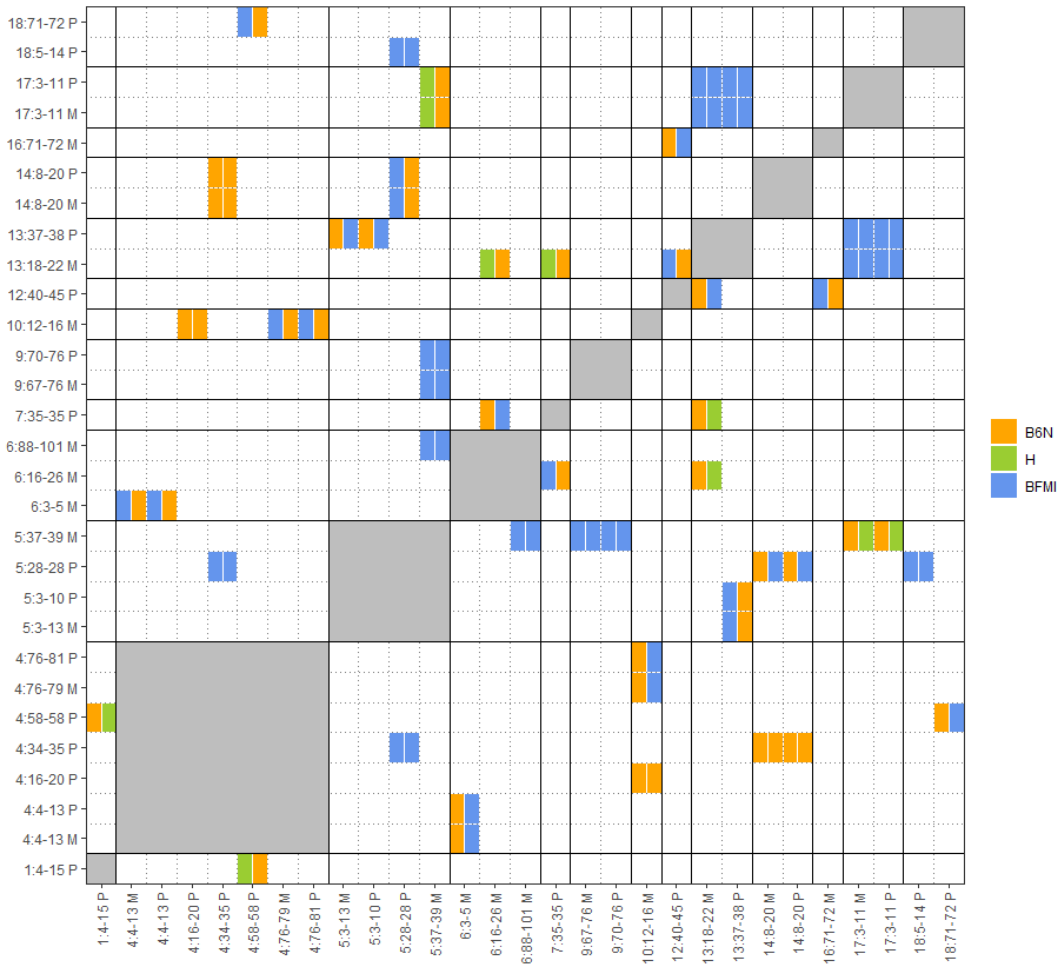

328 ## *Conclusions and discussion*

329 In this study, we examined an AIL population originating from a cross between the obese mouse line
330 BFMI and the standard mouse line B6N in generations 26 to 28 for TRD from parents and grandparents
331 to offspring. The most significant finding of this study was the detection of 62 genomic regions showing
332 TRD in the genotype data from generations 27 to 28.

333 We considered three possible explanations for the widespread TRD we observe in our AIL, (1)
334 independent selection at each locus, (2) gametic or meiotic drive, and (3) preferential selection of
335 combinations of alleles at two or more loci.

336 The first hypothesis that selection happens at each locus independently will often lead to
337 nonproductive crosses and/or massive lethality after birth (Huang et al. 2013a). The argument against
338 this first hypothesis is that the litter size in generation 28 does not deviate from the litter size in the
339 parental inbred lines BFMI and B6N (data not shown). When incompatibilities are (embryonically)
340 lethal this would cause a side-effect of significant TRD which should also be detectable as deviation
341 from the Hardy Weinberg equilibrium (HWE) in the offspring generation (Paterson et al. 2009). Since
342 regions out of HWE were excluded in our study, (embryonically) lethal alleles were not investigated in
343 our AIL. This means that the observed TRD cannot be due to lethality, leading us to reject this
344 hypothesis of direct independent selection at each locus as the cause for the TRD observed in our AIL.

345 The second possible mechanism for the TRD observed in this paper are the well-investigated examples
346 in mouse from meiotic drive, such as the *t*-complex (Safronova and Chubykin 2013). In short, meiotic
347 drive can be thought of as a conflict in which a selfish allele is able to use asymmetric meiosis in order
348 to have a greater chance of being transmitted to the gamete. This mechanism in first instance fits our
349 observations well, since peri-centromeric regions seem to be involved. Detected TRD regions in our
350 AIL were observed located in close proximity to the telocentric centromere for 10 out of 19 autosomes.
351 This observation is consistent with previous findings in e.g. *Drosophila,* where autosomal meiotic
352 drivers, occur in heterochromatic regions around centromere and telomere (Brand et al. 2015). In

353 mice, genetic incompatibilities in and around the centromeric regions between *Mus musculus*
354 *musculus* and *Mus musculus domesticus* have been known for decades (Fel-Clair et al. 1998;
355 Lenormand et al. 1997) and have been studied extensively in mouse populations near the hybrid zone
356 (Teeter et al. 2008; Larson et al. 2018). Centromere strength differs between mouse strains and was
357 found to predict the direction of meiotic drive in mice (Chmátal et al. 2014). Earlier findings showed
358 no incompatibility between the chromosome 11 centromere region in hybrids between *Mus musculus*
359 *musculus* and *Mus musculus domesticus* (Lanneluc et al. 2004). Our study confirms this finding, since
360 we also did not observe TRD at the chromosome 11 centromeric region. Genome-wide DNA
361 sequencing showed that BFMI is a hybrid between *Mus musculus musculus* and *Mus musculus*
362 *domesticus* (data not shown, sequencing data available at SRA*)*. As such, the AIL between BFMI and
363 B6N might have revived incompatibilities stemming from meiotic drive between *musculus* and
364 *domesticus* alleles. However, an argument against meiotic drive causing our TRD is that true meiotic
365 drive would have led to fixation of the favored allele / haplotype within 26 to 28 generations (Kursel
366 and Malik 2018). Since we do not observe this fixation, the meiotic drive hypothesis is unlikely to
367 underly the widespread TRD observed in our AIL. Additionally, in mammals only female meiosis was
368 found to be asymmetric (Brunet and Verlhac 2011; Kursel and Malik 2018), meaning that our observed
369 paternal TRD is most likely not due to meiotic drive. However, we cannot exclude that this hypothesis
370 might play a role for the maternal TRD regions observed near the centromeric regions. Furthermore,
371 pathway overrepresentation analysis does show overrepresentation of pathways which point to
372 meiotic drive in maternal BFMI TRD regions.

373 The third hypothesis is that TRD at each locus is not independent but rather caused by selection on
374 preferential combinations of alleles or selection against detrimental allele combinations (Martin-
375 DeLeon et al. 2005; Xie et al. 2019). nsSNPs in protein-coding genes located in TRD regions were
376 investigated to see if this hypothesis could explain the TRD observed. In total, we found 182 nsSNPs in
377 128 genes within the 62 identified regions showing TRD. Based on permutation we would have
378 expected to see only 125.9 ± 17.0 nsSNPs. The density of nsSNPs in genes in TRD regions was 44.5%

379 higher than expected by chance. While the changes in amino acid sequence derived from nsSNPs in a
380 single gene might not be sufficient to cause lethality or to reduce fitness, co-occurrence with SNPs in
381 protein-protein interaction partners could cause such adverse effects, e.g. by affecting protein-protein
382 binding leading to signaling problems (Xie et al. 2019). Such adverse effects could result in detectable
383 TRD. On evolutionary time scales this is known as protein co-evolution, known to leave detectable
384 footprints (Clark et al. 2011; Teppa et al. 2017). We hypothesize that this is what drives most TRD in
385 our BFMI x B6N AIL. In our AIL we combine the genome of BFMI (a mix between *Mus musculus*
386 *musculus* and *Mus musculus domesticus*) with B6N, a *Mus musculus musculus*. Our AIL as such forces
387 together the evolutionary separated genomes of *Mus musculus musculus* and *Mus musculus*
388 *domesticus* which might lead to resurging incompatibilities between proteins coded in different TRD
389 regions.

390 However, it should be noted that in this paper we did not investigate the subspecific origin of the TRD
391 regions and as such we can only hypothesize that protein-protein incompatibilities might be the
392 underlying mechanism for the TRD we observe. Further research on the subspecific origin of the TRD
393 would allow us to disentangle the contribution of each of the three hypotheses on our observed TRD.

394 Pairwise testing of genetic incompatibilities between the 62 identified TRD regions showed 29
395 genome-wide highly significant genetic incompatibilities in our AIL. Although our analysis shows that
396 observed allele TRD is likely due to incompatibility between proteins in two or more TRD regions,
397 genetic incompatibilities only account around half of TRD observed. Potentially, some incompatibilities
398 could not be detected since (1) we limited our analyses to pairwise testing TRD regions, (2)
399 incompatibilities might not always lead to detectable transmission ratio distortion, and (3) not all
400 protein-protein interactions are known yet and/or stored in the STRING database. Furthermore, some
401 genomic regions did not contain informative markers, and as such, they did not allow us to test for TRD
402 in these regions. However, we cannot exclude meiotic drive for maternal TRD regions near the
403 centromeres which might act alongside the genetic incompatibility hypothesis.

404 Pathways overrepresented in maternal BFMI TRD regions strongly point to meiotic drive with pathways
405 such as: “DNA methylation”, “meiotic/meiosis regulation”, “Chromatin organization”, “Nucleosome
406 assembly”, and “Telomere Maintenance” overrepresented. This is in line with the meiotic drive
407 hypothesis being causal for some of the maternal TRD observed near the centromeres.

408 Paternal TRD regions showed overrepresentation of “Signaling by Wnt”, “Metabolism of lipids and
409 lipoproteins”, and “Retinol metabolism”. These pathways point to incompatibilities, and genes located
410 in TRD regions, such as acyl-CoA oxidase 2 (*Acox2*), fat binding proteins 4 and 5 (*Fabp4*, *Fabp5*), fatty
411 acid desaturase 2 (*Fads2*) and malic enzyme 1 (*Me1*) which are known to be involved in energy
412 partitioning and metabolism phenotypes in which the BFMI and B6N founders differ. Recent work on
413 the retina of BFMI mice has shown differences in the rhodopsin layer of BFMI vs. B6N mice, pointing
414 towards an impaired retina function in BFMI mice. Eyes of the BFMI showed definite characteristics of
415 retinal degeneration in terms of a dysfunction of the rhodopsin transport and a reduction in the outer
416 nuclear layer (ONL) thickness (Brockmann C. et al. 2017). This might explain why genes located in the
417 “Retinol metabolism” pathway come up as significantly overrepresented. Our TRD analysis identifies
418 genes within TRD regions that could be considered as possible candidate genes for retinal
419 degeneration in mice and humans.

420 When looking into pathways that were overrepresented while analyzing TRD genes with nsSNPs,
421 pathways such as “Cell Cycle”, “Metabolism of lipids and lipoproteins”, “Metabolism”, “Signaling by
422 Rho GTPases” show in both paternal as well as maternal TRD regions. This provides support for the
423 hypothesis that fundamental cell cycle and metabolic processes are affected by TRD and that selection
424 of major phenotypic differences (e.g. body weight and fat composition) shaped the allelic composition
425 of the genome of the founder inbred lines by different genetic requirements. These genetic
426 adaptations are necessary for the optimization of the genome to ensure fitness and reproduction
427 during the generation of inbred lines and might be what causes the observed TRD when founder
428 genomes are combined together.

429 Our study sheds new light on the TRD in a cross between different inbred mouse strains, the distinct
430 functioning of genomes in producing viable offspring, and provides a way to identify candidate genes
431 which could contribute to complex traits different between the founder strains (in our case obesity
432 and/or retinal functionality). The genes in the TRD regions provide new targets for investigating genetic
433 adaptation and modifying determinants of complex traits.

434 ## Materials and Methods

435 ### Mouse population

436 348 male mice of an advanced intercross line (AIL) in generation 28 as well as their 62 parents and 66
437 grandparents from generations 27 and 26 were genotyped. The AIL population originates from the
438 mapping population of a cross between a male mouse of the obese line BFMI860-12 (BFMI) and a
439 female of the lean line C57BL/6NCrl (B6N), that had been initially used to map the juvenile obesity
440 locus *jObes1* (Neuschl et al. 2010). Beginning in generation F_1, individuals were randomly mated to
441 mice from the same generation using the program RandoMate (Schmitt et al. 2009).

442 ### Husbandry conditions

443 All experimental treatments of animals were approved by the German Animal Welfare Authorities
444 (approval no. G0016/11). All mice were maintained under conventional conditions and a 12:12 h
445 light:dark cycle (lights on at 6:00 am) at a temperature of 22 ± 2 °C. Animals had *ad libitum* access to
446 food and water. To perform fine mapping of the obesity QTL (Arends et al. 2016), generation 28 was
447 fed with a rodent high-fat diet (HFD) containing 19.5 MJ/kg of metabolizable energy, 45% from fat,
448 24% from protein and 31% from carbohydrates (E15103-34, ssniff EF R/M, Ssniff Spezialdiäten GmbH,
449 Soest / Germany). All other generations used in this study were fed a standard breeding diet (V1534-
450 000, ssniff EF R/M; Ssniff Spezialdiäten GmbH, Soest, Germany).

451 ### Genotypes

452 Genotypes were generated at GeneSeek (Lincoln, NE, USA) using the Mega Mouse Universal
453 Genotyping Array (MegaMUGA). These arrays are SNP genotyping arrays based on the Illumina
454 Infinium platform designed by investigators at the University of North Carolina at Chapel Hill,
455 manufactured by Illumina (San Diego, CA), and distributed by Neogen Inc (Lansing, MI, USA) (Morgan
456 and Welsh 2015). This array contains probes targeting 77,800 known SNPs. SNP probes were remapped
457 to the reference genome (GRCm38_95) using BLASTN with default settings (Camacho et al. 2009). In
458 order to increase the certainty of genotype calls, genotypes with a GenCall score greater than 0.7 were

459 considered confidently called, although the manufacturer's recommendation is a GenCall score > 0.15.
460 SNPs that mapped to multiple positions in the genome, non-informative SNPs, and SNPs with genotype
461 call rates below 90% were removed from further analysis. In total, 14,415 highly confident SNPs passed
462 all quality checks and were informative between BFMI and B6N. Marker density, as well as minor allele
463 frequencies (MAF) within and outside of TRD regions were visualized and can be found in
464 Supplemental_Table_S5.

465 Furthermore, checking parent-child relations in our trio data identified 3 individuals in generation 28
466 where one of the parents was wrongly assigned, these 3 individuals were removed from further
467 analysis. Similarly, one individual in generation 27 was found to have a wrong parent assignment,
468 leading to the removal of this individual and its 4 offspring in generation 28. Phasing of the
469 heterozygous genotypes of the AIL animals of generation 28 towards the parental population
470 (generation 27), and of generation 27 to generation 26 was done using Beagle v4.1 (Browning and
471 Browning 2007) with standard settings. Raw and phased genotypes of all individuals that passed
472 quality control ($N_{(28)}$ = 341, $N_{(27)}$ = 61, and $N_{(26)}$ = 66), the genetic map, and pedigree data are available
473 in Supplemental_Table_S2.

474 ***Allele transmission from heterozygous parents***

475 Deviations from expected Mendelian inheritance ratios are named transmission ratio distortion (TRD).
476 Such deviations have been commonly observed in experimental crosses as well as in natural
477 populations. We used an extension of the transmission asymmetry test and parental asymmetry test
478 to detect parent-of-origin dependent effects on the frequency of the transmission of a specific SNP
479 allele from parent to offspring using trios in our AIL design (Weinberg et al. 1998). For example: To
480 determine if one of the alternative paternal alleles (e.g. A versus B allele) at a SNP locus is inherited
481 more often than expected by Mendel (50%), pups were analyzed in generation 28 of fathers
482 (generation 27) that were heterozygous for this SNP. We only tested markers at which at least 10
483 heterozygous fathers (or mothers) were available. We counted the number of offspring where a
484 specific paternal allele was transmitted. When both parents were heterozygous, the allele transmitted

485 cannot be determined and this transmission was not counted in the test statistic. Furthermore,
486 markers were tested for Hardy Weinberg equilibrium (HWE) using the code developed by Wigginton
487 *et al.* (Wigginton et al. 2005). Markers not in HWE were excluded, since the χ^2 test for TRD is only valid
488 when a marker is in HWE. A χ^2 test was used to test if this distribution of paternally inherited alleles
489 significantly deviated from the expected Mendelian inheritance ratios (**Pat**), and similarly for
490 maternally inherited alleles (**Mat**).

491 - ***Pat***: Analysis of allele transmission ratio distortion from heterozygous fathers to offspring
492 $\chi^2_{Pat} = (P_{AB} - P_{BA})^2 / (P_{AB} + P_{BA})$
493 - ***Mat***: Analysis of allele transmission ratio distortion from heterozygous mothers to offspring
494 $\chi^2_{Mat} = (M_{AB} - M_{BA})^2 / (M_{AB} + M_{BA})$

495 χ^2 scores were transformed into p-values using the appropriate conversions and then transformed into
496 LOD scores using $-\log_{10}$(p-value). 5% and 1% significance thresholds were determined by Bonferroni
497 correction (5% >= 6.75, 1% >= 7.45). Significant regions were defined as the region from the first to the
498 last flanking marker above the 1% significance threshold (LOD scores >= 7.45).

499 ***Genetic variants in TRD regions***

500 Parental genomes (BFMI860-12 and B6N) were paired-end sequenced using the "Illumina HiSeq"
501 platform (Illumina Inc., San Diego, California, U.S.). Obtained DNA reads were trimmed using
502 trimmomatic (Bolger et al. 2014) after which trimmed reads were aligned to the mouse genome
503 (MM10, GRCm38.p6) using the Burrows–Wheeler Aligner (BWA) software (Li and Durbin 2009). The
504 subsequent SAM files were converted to BAM files, sorted, and indexed using Samtools (Li et al. 2009;
505 Morgan et al. 2017). (Optical) Duplicate reads were removed using Picard tools v2.19.0 (Broad Institute
506 2016), after which indel realignment and base recalibration was done using the GATK v4.1.0.0
507 (McKenna et al. 2010), according to GATK best practices (Broad Institute 2018). Sequence variants
508 were called using BCFtools (Morgan et al. 2017) Variants passing quality control were further
509 annotated using the Ensembl Variant Effect Predictor (VEP) (McLaren et al. 2016). DNA sequencing

510 data allowed to identify non-synonymous SNPs (nsSNPs) in genes located in TRD regions between the
511 founding strains.

512 A permutation strategy was used to detect over- and/or underrepresentation of nsSNPs in the regions
513 showing TRD. We performed 50,000 permutations, each time drawing 1,424 protein-coding genes at
514 random, not allowing duplicate genes or selection of predicted genes (GM/RIKEN). For every
515 permutation, the number of nsSNPs and the number of genes with nsSNPs was recorded. After 50,000
516 permutations, a distribution of the total number of nsSNPs (and genes) in the random data was
517 obtained, which was compared with the observed data.

518 ***Pathway overrepresentation analyses***

519 We extracted all protein-coding genes inside the significant regions using biomaRt (Kasprzyk 2011) for
520 each of the different types of allele transmission ratio distortion: Preferred paternal transmission of
521 the BFMI allele (Pat_BFMI), preferred paternal transmission of the B6N allele (Pat_B6N), preferred
522 maternal transmission of the BFMI allele (Mat_BFMI), and preferred maternal transmission of the B6N
523 allele (Mat_B6N). To identify potential functional clustering of genes within one of these groups,
524 pathway overrepresentation analyses was performed using innateDB (Breuer et al. 2013) with KEGG
525 (Ogata et al. 2000) and Reactome (Joshi-Tope et al. 2005) as the pathway providers.
526 Overrepresentation was tested using a hypergeometric test. P-values reported for pathway
527 overrepresentation were Benjamini-Hochberg corrected ($P_{(BH)}$) (Benjamini and Hochberg 1995); $P_{(BH)} <$
528 0.05 were considered significant. Pathway analysis was additionally performed with genes showing
529 nsSNPs using the same grouping as before, with "_SNP" added to the group identifier (Pat_BFMI_SNP,
530 Mat_BFMI_SNP, Pat_B6N_SNP, and Mat_B6N_SNP).

531 ***Genetic incompatibilities***

532 Testing for pairwise genetic incompatibilities in an exhaustive manner is not advisable because of the
533 large number of statistical tests required for 20k SNP markers leading to a severe multiple testing
534 correction. Our hypothesis is that genetic incompatibilities cause allele transmission ratio distortions.

535 For testing incompatibilities, 3x3 contingency tables were created using the top SNP marker in the TRD
536 region 1 (M1) versus the top SNP marker in TRD region 2 (M1), and the number of co-occurrences
537 between different alleles was counted. If no top marker was present in a region e.g. Pat_R5, due to all
538 markers showing a similar distortion, the proximal flanking marker was used as top marker. Our
539 method for scoring genetic incompatibility is very similar to the methods used by Ackermann and Beyer
540 and Corbett-Detig et al (Ackermann and Beyer 2012; Corbett-Detig et al. 2013). A 3x3 table of expected
541 co-occurrences based on the observed allele frequencies at markers M1 and M2 was generated
542 assuming independent segregation of each marker. Resulting χ^2 scores were transformed into p-
543 values, which are then transformed to LOD scores as described before. For each pair of markers that
544 showed a genome-wide significant interaction ($P_{(BF)} < 0.05$), founder alleles of the group which shows
545 the most reduction (in percentage) between observed and expected co-occurrences was used for the
546 visualization seen in Figure 2.

547 Pairwise interactions tests were only performed between detected TRD regions, while correction for
548 multiple testing was done using genome-wide thresholds. This first involved estimating the number of
549 effective tests by using the simpleM method (Gao 2011). The simpleM method was designed to
550 estimate the number of independent tests in a GWAS by considering linkage between markers. The
551 simpleM procedure estimated 1,008 independent test (at a fixLength of 1200) which is much lower
552 than the number of genetic markers. This reduction in total tests can be explained by strong linkage
553 between markers in our AIL population. LOD thresholds were adjusted for multiple testing using
554 Bonferroni correction ($P_{(BF)}$) and the number of independent tests estimated with the simpleM method
555 (n=1,008). Since we tested pairwise but without repeating the test for a pair we have already tested,
556 the number of tests had to be multiplied with itself and reduced by half leading to LOD scores
557 calculated as: -log10(threshold / (1,008 * 1,008 * 0.5). Dependent on the significance threshold, this
558 leads to the following genome-wide adjusted LOD thresholds: significant if LOD > 7.0 ($P_{(BF)} < 0.05$) and
559 highly significant if LOD > 7.7 ($P_{(BF)} < 0.01$).

560 We then continued our investigation of known protein-protein interactions between genes with non-
561 synonymous SNPs (nsSNPs) within these regions of incompatibility using the Search Tool for the
562 Retrieval of Interacting Genes/Proteins (STRING) database version 11 (Szklarczyk et al. 2019). In total
563 9,602,772 known physical protein-protein interactions for *Mus musculus* (SpeciesID 10090) are listed
564 in this database (10090.protein.physical.links.v11.0). We first only considered the protein-protein
565 interactions between the 128 genes with one or more nsSNP(s). Afterwards, we overlaid the gene
566 location data with the TRD regions for which we found genome-wide significant evidence of genetic
567 incompatibilities. This was done to see if identified genetic compatibility could be explained by known
568 physical protein-protein interactions in which both participating genes show one or more nsSNP(s).

569 *List of abbreviations*

570 AIL - Advanced intercross line

571 BFMI - Berlin Fat Mouse inbred line

572 B6N - C57BL/6N inbred line

573 Mat - Maternal transmission ratio distortion

574 MAF – Minor allele frequency

575 nsSNP - Non-Synonymous Single Nucleotide Polymorphism

576 $P_{(BF)}$ - Bonferroni corrected p-value

577 $P_{(BH)}$ - Benjamini–Hochberg corrected p-value

578 Pat - Paternal transmission ratio distortion

579 QTL - Quantitative trait locus

580 SNP - Single nucleotide polymorphism

581 TRD - Transmission ratio distortion

Declarations

Ethics approval

All experimental treatments of animals were approved by the German Animal Welfare Authorities (approval no. G0016/11).

Availability of data and materials

The datasets supporting the conclusions of this article are included within the article and its supplementary files. DNA sequencing data was deposited at the NCBI Sequence Read Archive (SRA) under BioProject ID: PRJNA717237

Conflict of Interest

The authors declare no conflict of interest.

Funding

The project was funded by the Deutsche Forschungsgemeinschaft (DFG) (BR 1285/12-2).

Authors' contributions

D.A. contributed to the design of the experiment, performed the data analysis and drafted the manuscript. **S. K.** was involved in the design of the experiment, animal handling, sample collection, and contributed to the manuscript. **S.H.** was responsible for animal handling, sample collection and DNA extraction. **P.K.** contributed to critical data analysis discussions, revision of the manuscript and Table 1, and Figure 2. **D.H.** contributed to writing and critical revision of the manuscript, and discussion about the biological implications of the observed TRD. **G.A.B.** designed the experiment, planned, organized and supervised the project; contributed to write and critically revise the manuscript.

Authors' information

Dr. Danny Arends finished his PhD at the Groningen Bioinformatics Centre at the University of Groningen in November 2014 and is currently working as a PostDoc at the Humboldt University in Berlin. He develops new computational methodologies and open source software for use in (systems) biology research, such as the addition of Multiple QTL Mapping (MQM) into R/qtl. His focus is development of large-scale computational methods in QTL analysis, and the integration of 'big data' biological data sets in a comprehensive manner.

Dr. Sebastian Heise finished his PhD in the group Breeding Biology and molecular Genetics at Humboldt-University in Berlin in November 2014. He is working with lean and obese mouse models on projects focusing on insulin sensitivity and type-2 diabetes. Exploring the genetics contribution beyond the complex traits is the key interest of his projects.

Dr. Stefan Kärst finished his PhD in the group Breeding Biology and molecular Genetics at Humboldt-University in Berlin in October 2011 and is currently working at a Biotech company in Berlin. During his PhD and PostDoc at the Humboldt University in Berlin, Stefan developed new methods for phenotyping, mapped muscle trait QTLs and analyzed NGS data for gene expression and sequence variants.

618 Dr. Paula Korkuc obtained her Bioinformatics Ph.D. degree from the University of Potsdam in
619 cooperation with the Max-Planck institute for Molecular Plant Physiology in 2016. She is currently
620 working as a PostDoc at the Humboldt University in Berlin. Her current research focusses on the
621 identification of functional variants associated with milk production traits in the endangered German
622 DSN cattle breed using DNA sequencing, SNP-chip data, and novel computational methods
623 implemented in R.

624 Dr. Deike Hesse studied biology at the universities of Düsseldorf, Nantes and Marburg. She obtained
625 her doctor degree from the University of Potsdam in collaboration with the German Institute for
626 Human Nutrition in 2010. Since 2017 she works as a researcher and lecturer at the Humboldt
627 University in Berlin. Her research focusses on energy metabolism, body weight development, and
628 diabetes. Using mouse models with different genetic backgrounds she aims to elucidate the
629 contribution and interaction of different tissues and metabolic pathways to metabolic phenotypes.

630 Prof. Dr. Gudrun A. Brockmann studied Biophysics in Berlin, finished her PhD in Embryology at the
631 Academy of Agricultural Sciences, and obtained her Habilitation in the field of Genetics at Rostock
632 University, Germany. She had worked with mice as models for animal breeding at the Leibnitz-
633 Institute for Farm Animals in Dummerstorf, before she was appointed as a Full Professor for Animal
634 Breeding and Molecular Genetics at Humboldt-University Berlin in 2003. Her interest is the
635 understanding of genetics underlying complex traits with a focus on energy partitioning. She is
636 author of more than 130 papers, acts on scientific advisory boards, and as reviewer for all kind of
637 research applications.

638 ## *References*

639 Ackermann M, Beyer A. 2012. Systematic Detection of Epistatic Interactions Based on Allele Pair
640 Frequencies ed. J. Flint. *PLoS Genet* **8**: e1002463.
641 https://dx.plos.org/10.1371/journal.pgen.1002463.

642 Arends D, Heise S, Kärst S, Trost J, Brockmann GA. 2016. Fine mapping a major obesity locus (jObes1)
643 using a Berlin Fat Mouse × B6N advanced intercross population. *Int J Obes* **40**: 1784–1788.
644 http://www.nature.com/articles/ijo2016150.

645 Benjamini Y, Hochberg Y. 1995. Controlling the False Discovery Rate: A Practical and Powerful
646 Approach to Multiple Testing. *J R Stat Soc Ser B* **57**: 289–300.
647 http://www.jstor.org/stable/pdfplus/2346101.pdf?acceptTC=true.

648 Blake JA, Baldarelli R, Kadin JA, Richardson JE, Smith CL, Bult CJ, Anagnostopoulos A V, Beal JS, Bello
649 SM, Blodgett O, et al. 2021. Mouse Genome Database (MGD): Knowledgebase for mouse–
650 human comparative biology. *Nucleic Acids Res* **49**: D981–D987.
651 https://academic.oup.com/nar/article/49/D1/D981/5999894.

652 Bolger AM, Lohse M, Usadel B. 2014. Trimmomatic: a flexible trimmer for Illumina sequence data.
653 *Bioinformatics* **30**: 2114–2120.
654 http://bioinformatics.oxfordjournals.org/content/30/15/2114%5Cnhttp://bioinformatics.oxford
655 journals.org/content/30/15/2114.abstract.html?etoc%5Cnhttp://bioinformatics.oxfordjournals.
656 org/content/30/15/2114.full.pdf%5Cnhttp://www.ncbi.nlm.nih.gov/pubmed/24695404
657 (Accessed July 9, 2014).

658 Brand CL, Larracuente AM, Presgraves DC. 2015. Origin, evolution, and population genetics of the
659 selfish Segregation Distorter gene duplication in European and African populations of
660 Drosophila melanogaster. *Evolution (N Y)*.

661 Breuer K, Foroushani AK, Laird MR, Chen C, Sribnaia A, Lo R, Winsor GL, Hancock REW, Brinkman FSL,
662 Lynn DJ. 2013. InnateDB: Systems biology of innate immunity and beyond - Recent updates and

663 continuing curation. *Nucleic Acids Res* **41**.

664 Broad Institute. 2018. GATK Best Practices. https://software.broadinstitute.org/gatk/best-practices/
665 (Accessed February 1, 2018).

666 Broad Institute. 2016. Picard tools. https://broadinstitute.github.io/picard/.

667 Brockmann C., Brockmann T., Dege S., Skosyrski S., Strauß O, Joussen A. M. 2017. SaF08-04 -
668 Hereditäre Retinale Degeneration der Berliner Fettmaus. In *Abstractband DOG*, p. 201
669 https://www.dog.org/wp-content/uploads/2017/08/Abstractband_DOG_2017.pdf.

670 Browning SR, Browning BL. 2007. Rapid and accurate haplotype phasing and missing-data inference
671 for whole-genome association studies by use of localized haplotype clustering. *Am J Hum Genet*
672 **81**: 1084–1097.

673 Brunet S, Verlhac MH. 2011. Positioning to get out of meiosis: The asymmetry of division. *Hum*
674 *Reprod Update*.

675 Buniello A, MacArthur JAL, Cerezo M, Harris LW, Hayhurst J, Malangone C, McMahon A, Morales J,
676 Mountjoy E, Sollis E, et al. 2019. The NHGRI-EBI GWAS Catalog of published genome-wide
677 association studies, targeted arrays and summary statistics 2019. *Nucleic Acids Res* **47**: D1005–
678 D1012. https://academic.oup.com/nar/article/47/D1/D1005/5184712.

679 Camacho C, Coulouris G, Avagyan V, Ma N, Papadopoulos J, Bealer K, Madden TL. 2009. BLAST+:
680 architecture and applications. *BMC Bioinformatics* **10**: 421.

681 Chmátal L, Gabriel SI, Mitsainas GP, Martínez-Vargas J, Ventura J, Searle JB, Schultz RM, Lampson
682 MA. 2014. Centromere strength provides the cell biological basis for meiotic drive and
683 karyotype evolution in mice. *Curr Biol*.

684 Clark GW, Dar V-N, Bezginov A, Yang JM, Charlebois RL, Tillier ERM. 2011. Using Coevolution to
685 Predict Protein–Protein Interactions. pp. 237–256 http://link.springer.com/10.1007/978-1-
686 61779-276-2_11.

687 Comuzzie AG, Cole SA, Laston SL, Voruganti VS, Haack K, Gibbs RA, Butte NF. 2012. Novel Genetic
688 Loci Identified for the Pathophysiology of Childhood Obesity in the Hispanic Population. *PLoS*
689 *One*.

690 Corbett-Detig RB, Zhou J, Clark AG, Hartl DL, Ayroles JF. 2013. Genetic incompatibilities are
691 widespread within species. *Nature* **504**: 135–7.
692 http://www.ncbi.nlm.nih.gov/pubmed/24196712.

693 DeBosch BJ, Kluth O, Fujiwara H, Schürmann A, Moley K. 2014. Early-onset metabolic syndrome in
694 mice lacking the intestinal uric acid transporter SLC2A9. *Nat Commun* **5**: 4642.
695 http://www.nature.com/articles/ncomms5642.

696 Dinour D, Gray NK, Campbell S, Shu X, Sawyer L, Richardson W, Rechavi G, Amariglio N, Ganon L, Sela
697 BA, et al. 2010. Homozygous SLC2A9 mutations cause severe renal hypouricemia. *J Am Soc*
698 *Nephrol*.

699 Duriez B, Duquesnoy P, Escudier E, Bridoux AM, Escalier D, Rayet I, Marcos E, Vojtek AM, Bercher JF,
700 Amselem S. 2007. A common variant in combination with a nonsense mutation in a member of
701 the thioredoxin family causes primary ciliary dyskinesia. *Proc Natl Acad Sci U S A*.

702 Fel-Clair F, Catalan J, Lenormand T, Britton-Davidian J. 1998. Centromeric Incompatibilities in the
703 Hybrid Zone Between House Mouse Subspecies from Denmark: Evidence from Patterns of Nor
704 Activity. *Evolution (N Y)* **52**: 592–603.

705 Fischer E, Charbonneau H, Tonks N. 1991. Protein tyrosine phosphatases: a diverse family of
706 intracellular and transmembrane enzymes. *Science (80-)* **253**: 401–406.
707 https://www.sciencemag.org/lookup/doi/10.1126/science.1650499.

708 Fitzpatrick JL, Evans JP. 2009. Reduced heterozygosity impairs sperm quality in endangered
709 mammals. *Biol Lett* **5**: 320–323. https://royalsocietypublishing.org/doi/10.1098/rsbl.2008.0734.

710 Flurkey K, Currer JM, Leiter EH, Witham B, Jackson Laboratory (Bar Harbor M. 2009. *The Jackson*

711 *Laboratory Handbook on Genetically Standardized Mice*. 6th ed. eds. K. Flurkey, J.M. Currer,
712 E.H. Leiter, and B. Witham. The Jackson Laboratory, Bar Harbor, ME 04609 USA
713 https://www.urmc.rochester.edu/MediaLibraries/URMCMedia/animal-
714 resource/forms/documents/JAX-Handbook-Genetically-Standardized-Mice.pdf.

715 Gao X. 2011. Multiple testing corrections for imputed SNPs. *Genet Epidemiol* **35**: 154–158.

716 GeneCards Human Gene Database. 2021. STK32B Gene - GeneCards. https://www.genecards.org/cgi-
717 bin/carddisp.pl?gene=STK32B.

718 Heid IM, Jackson AU, Randall JC, Winkler TW, Qi L, Steinthorsdottir V, Thorleifsson G, Zillikens MC,
719 Speliotes EK, Mägi R, et al. 2010. Meta-analysis identifies 13 new loci associated with waist-hip
720 ratio and reveals sexual dimorphism in the genetic basis of fat distribution. *Nat Genet* **42**: 949–
721 960. https://www.nature.com/articles/ng.686.pdf.

722 Heinonen S, Buzkova J, Muniandy M, Kaksonen R, Ollikainen M, Ismail K, Hakkarainen A, Lundbom J,
723 Lundbom N, Vuolteenaho K, et al. 2015. Impaired mitochondrial biogenesis in adipose tissue in
724 acquired obesity. *Diabetes*.

725 Hirsch CN, Flint-Garcia SA, Beissinger TM, Eichten SR, Deshpande S, Barry K, McMullen MD, Holland
726 JB, Buckler ES, Springer N, et al. 2014. Insights into the Effects of Long-Term Artificial Selection
727 on Seed Size in Maize. *Genetics* **198**: 409–421.
728 https://academic.oup.com/genetics/article/198/1/409-421/6073421.

729 Huang LO, Labbe A, Infante-Rivard C. 2013a. Transmission ratio distortion: review of concept and
730 implications for genetic association studies. *Hum Genet* **132**: 245–63.
731 http://www.ncbi.nlm.nih.gov/pubmed/23242375.

732 Huang X, Baumann M, Nikitina L, Wenger F, Surbek D, Körner M, Albrecht C. 2013b. RNA degradation
733 differentially affects quantitative mRNA measurements of endogenous reference genes in
734 human placenta. *Placenta* **34**: 544–7. http://www.ncbi.nlm.nih.gov/pubmed/23623484
735 (Accessed October 11, 2013).

736 Joshi-Tope G, Gillespie M, Vastrik I, D'Eustachio P, Schmidt E, de Bono B, Jassal B, Gopinath GR, Wu
737 GR, Matthews L, et al. 2005. Reactome: a knowledgebase of biological pathways. *Nucleic Acids*
738 *Res* **33**: D428-32. http://www.ncbi.nlm.nih.gov/pubmed/15608231.

739 Kasprzyk A. 2011. BioMart: driving a paradigm change in biological data management. *Database*
740 *(Oxford)* **2011**: bar049.
741 http://www.pubmedcentral.nih.gov/articlerender.fcgi?artid=3215098&tool=pmcentrez&render
742 type=abstract (Accessed July 12, 2014).

743 Klink BU, Gatsogiannis C, Hofnagel O, Wittinghofer A, Raunser S. 2020. Structure of the human
744 BBSome core complex. *Elife* **9**. https://elifesciences.org/articles/53910.

745 Kopelman P. 2007. Health risks associated with overweight and obesity. *Obes Rev* **8**: 13–17.
746 http://doi.wiley.com/10.1111/j.1467-789X.2007.00311.x.

747 Kursel LE, Malik HS. 2018. The cellular mechanisms and consequences of centromere drive. *Curr Opin*
748 *Cell Biol*.

749 Lanneluc I, Desmarais E, Boursot P, Dod B, Bonhomme F. 2004. Characterization of a centromeric
750 marker on mouse Chromosome 11 and its introgression in a domesticus/musculus hybrid zone.
751 *Mamm Genome*.

752 Larson EL, Vanderpool D, Sarver BAJ, Callahan C, Keeble S, Provencio LL, Kessler MD, Stewart V,
753 Nordquist E, Dean MD, et al. 2018. The evolution of polymorphic hybrid incompatibilities in
754 house mice. *Genetics*.

755 Lenormand T, Fel-Clair F, Manolakou K, Alibert P, Britton-Davidian J. 1997. Chromosomal
756 transmission bias in laboratory hybrids between wild strains of the two European subspecies of
757 house mice. *Genetics*.

758 Li G, Jin J, Zhou Y, Bai X, Mao D, Tan C, Wang G, Ouyang Y. 2019. Genome-wide dissection of
759 segregation distortion using multiple inter-subspecific crosses in rice. *Sci China Life Sci* **62**: 507–

760 516. http://link.springer.com/10.1007/s11427-018-9452-8.

761 Li H, Durbin R. 2009. Fast and accurate short read alignment with Burrows-Wheeler transform.
762 *Bioinformatics* **25**: 1754–60. https://www.ncbi.nlm.nih.gov/pmc/articles/PMC2705234/
763 (Accessed July 9, 2014).

764 Li H, Handsaker B, Wysoker A, Fennell T, Ruan J, Homer N, Marth G, Abecasis GR, Durbin R. 2009. The
765 Sequence Alignment/Map format and SAMtools. *Bioinformatics* **25**: 2078–2079.
766 https://academic.oup.com/bioinformatics/article-lookup/doi/10.1093/bioinformatics/btp352.

767 Locke AE, Kahali B, Berndt SI, Justice AE, Pers TH, Day FR, Powell C, Vedantam S, Buchkovich ML, Yang
768 J, et al. 2015. Genetic studies of body mass index yield new insights for obesity biology. *Nature*
769 **518**: 197–206. http://dx.doi.org/10.1038/nature14177.

770 Lu M, Varley AW, Ohta S, Hardwick J, Munford RS. 2008. Host Inactivation of Bacterial
771 Lipopolysaccharide Prevents Prolonged Tolerance Following Gram-Negative Bacterial Infection.
772 *Cell Host Microbe* **4**: 293–302.
773 https://linkinghub.elsevier.com/retrieve/pii/S1931312808002242.

774 Lyon MF. 2003. Transmission ratio distortion in mice. *Annu Rev Genet* **37**: 393–408.
775 http://www.ncbi.nlm.nih.gov/pubmed/14616067.

776 Martin-DeLeon PA, Zhang H, Morales CR, Zhao Y, Rulon M, Barnoski BL, Chen H, Galileo DS. 2005.
777 Spam I-associated transmission ratio distortion in mice: Elucidating the mechanism. *Reprod Biol*
778 *Endocrinol*.

779 Matsuo H, Chiba T, Nagamori S, Nakayama A, Domoto H, Phetdee K, Wiriyasermkul P, Kikuchi Y, Oda
780 T, Nishiyama J, et al. 2008. Mutations in Glucose Transporter 9 Gene SLC2A9 Cause Renal
781 Hypouricemia. *Am J Hum Genet*.

782 McKenna A, Hanna M, Banks E, Sivachenko AY, Cibulskis K, Kernytsky AM, Garimella K, Altshuler D,
783 Gabriel S, Daly MJ, et al. 2010. The Genome Analysis Toolkit: A MapReduce framework for

784 analyzing next-generation DNA sequencing data. *Genome Res* **20**: 1297–1303.
785 http://genome.cshlp.org/cgi/doi/10.1101/gr.107524.110 (Accessed July 9, 2014).

786 McLaren W, Gil L, Hunt SE, Riat HS, Ritchie GRS, Thormann A, Flicek P, Cunningham F. 2016. The
787 Ensembl Variant Effect Predictor. *Genome Biol* **17**: 1–14.

788 Morgan AP, Welsh CE. 2015. Informatics resources for the Collaborative Cross and related mouse
789 populations. *Mamm Genome*.

790 Morgan M, Pagès H, Obenchain V, N H. 2017. Rsamtools: Binary alignment (BAM), FASTA, variant call
791 (BCF), and tabix file import. *R Packag version 1300*.
792 http://bioconductor.org/packages/release/bioc/html/Rsamtools.html (Accessed February 15,
793 2018).

794 Mouse Genome Database (MGD). 2021. Myo5c - MGI Mouse Gene Detail.
795 http://www.informatics.jax.org/marker/MGI:2442485 (Accessed September 3, 2021).

796 Neuschl C, Hantschel C, Wagener A, Schmitt AO, Illig T, Brockmann GA. 2010. A unique genetic defect
797 on chromosome 3 is responsible for juvenile obesity in the Berlin Fat Mouse. *Int J Obes* **34**:
798 1706–1714. https://www.nature.com/articles/ijo201097.

799 Ogata H, Goto S, Sato K, Fujibuchi W, Bono H, Kanehisa M, Goto S. 2000. KEGG: kyoto encyclopedia
800 of genes and genomes. *Nucleic Acids Res* **28**: 29–34.
801 https://www.ncbi.nlm.nih.gov/pmc/articles/PMC102409/.

802 Ojogun NI. 2008. CONSTITUTIVE OVEREXPRESSION OF ACYLOXYACYL HYDROLASE IN MUS
803 MUSCULUS. The University of Texas Southwestern Medical Center at Dallas https://utswmed-
804 ir.tdl.org/bitstream/handle/2152.5/383/OjogunNoredia.pdf.

805 Papes F, Kemper EL, Cord-Neto G, Langone F, Arruda P. 1999. Lysine degradation through the
806 saccharopine pathway in mammals: involvement of both bifunctional and monofunctional
807 lysine-degrading enzymes in mouse. *Biochem J* **344 Pt 2**: 555–63.

808 https://portlandpress.com/biochemj/article/344/2/555/36179/Lysine-degradation-through-
809 the-saccharopine.

810 Paterson AD, Waggott D, Schillert A, Infante-Rivard C, Bull SB, Yoo YJ, Pinnaduwage D. 2009.
811 Transmission-ratio distortion in the Framingham Heart Study. *BMC Proc* **3**: S51.
812 https://bmcproc.biomedcentral.com/articles/10.1186/1753-6561-3-S7-S51.

813 Rodríguez-Carrizalez AD, Castellanos-González JA, Martínez-Romero EC, Miller-Arrevillaga G, Villa-
814 Hernández D, Hernández-Godínez PP, Ortiz GG, Pacheco-Moisés FP, Cardona-Muñoz EG,
815 Miranda-Díaz AG. 2014. Oxidants, antioxidants and mitochondrial function in non-proliferative
816 diabetic retinopathy. *J Diabetes*.

817 Rodriguez OC, Cheney RE. 2002. Human myosin-Vc is a novel class V myosin expressed in epithelial
818 cells. *J Cell Sci*.

819 Sacksteder KA, Biery BJ, Morrell JC, Goodman BK, Geisbrecht B V., Cox RP, Gould SJ, Geraghty MT.
820 2000. Identification of the α-aminoadipic semialdehyde synthase which is defective in familial
821 hyperlysinemia. *Am J Hum Genet*.

822 Safronova LD, Chubykin VL. 2013. Meiotic drive in mice carrying t-complex in their genome. *Russ J*
823 *Genet*.

824 Schmitt AO, Bortfeldt RH, Neuschl C, Brockmann GA. 2009. RandoMate: A program for the
825 generation of random mating schemes for small laboratory animals. *Mamm Genome* **20**: 321–
826 325.

827 Shungin D, Winkler TW, Croteau-Chonka DC, Ferreira T, Locke AE, Mägi R, Strawbridge RJ, Pers TH,
828 Fischer K, Justice AE, et al. 2015. New genetic loci link adipose and insulin biology to body fat
829 distribution. *Nature* **518**: 187–96. http://dx.doi.org/10.1038/nature14132.

830 Singhai M, Goyal R, Faizy A. 2011. Glutathione peroxidase activity in obese and nonobese diabetic
831 patients and role of hyperglycemia in oxidative stress. *J Midlife Health*.

832 Speliotes EK, Willer CJ, Berndt SI, Monda KL, Thorleifsson G, Jackson AU, Allen HL, Lindgren CM, Luan
833 J, Mägi R, et al. 2010. Association analyses of 249,796 individuals reveal 18 new loci associated
834 with body mass index. *Nat Genet* **42**: 937–948. https://www.nature.com/articles/ng.686.pdf.

835 Szklarczyk D, Gable AL, Lyon D, Junge A, Wyder S, Huerta-Cepas J, Simonovic M, Doncheva NT, Morris
836 JH, Bork P, et al. 2019. STRING v11: Protein-protein association networks with increased
837 coverage, supporting functional discovery in genome-wide experimental datasets. *Nucleic Acids*
838 *Res*.

839 Teeter KC, Payseur BA, Harris LW, Bakewell MA, Thibodeau LM, O'Brien JE, Krenz JG, Sans-Fuentes
840 MA, Nachman MW, Tucker PK. 2008. Genome-wide patterns of gene flow across a house
841 mouse hybrid zone. *Genome Res* **18**: 67–76.

842 Temtamy SA, Aglan MS, Valencia M, Cocchi G, Pacheco M, Ashour AM, Amr KS, Helmy SMH, El-
843 Gammal MA, Wright M, et al. 2008. Long interspersed nuclear element-1 (LINE1)-mediated
844 deletion of EVC, EVC2, C4orf6, and STK32B in ellis-van Creveld syndrome with borderline
845 intelligence. *Hum Mutat*.

846 Teppa E, Zea DJ, Marino-Buslje C. 2017. Protein–protein interactions leave evolutionary footprints:
847 High molecular coevolution at the core of interfaces. *Protein Sci*.

848 Tremmel M, Gerdtham U-G, Nilsson P, Saha S. 2017. Economic Burden of Obesity: A Systematic
849 Literature Review. *Int J Environ Res Public Health* **14**: 435. http://www.mdpi.com/1660-
850 4601/14/4/435.

851 Wagener A, Schmitt AO, Aksu S, Schlote W, Neuschl C, Brockmann GA. 2006. Genetic, sex, and diet
852 effects on body weight and obesity in the Berlin Fat Mouse Inbred lines. *Physiol Genomics* **27**:
853 264–270.

854 Weinberg CR, Wilcox AJ, Lie RT. 1998. A log-linear approach to case-parent-triad data: assessing
855 effects of disease genes that act either directly or through maternal effects and that may be
856 subject to parental imprinting. *Am J Hum Genet* **62**: 969–978.

857 Whitlock MC. 2000. Fixation Of New Alleles And The Extinction Of Small Populations: Drift Load,
858 Beneficial Alleles, And Sexual Selection. *Evolution (N Y)* **54**: 1855–1861.
859 http://doi.wiley.com/10.1111/j.0014-3820.2000.tb01232.x.

860 Wigginton JE, Cutler DJ, Abecasis GR. 2005. A Note on Exact Tests of Hardy-Weinberg Equilibrium.
861 *Am J Hum Genet* **76**: 887–893.
862 https://linkinghub.elsevier.com/retrieve/pii/S0002929707607356.

863 Willer CJ, Speliotes EK, Loos RJF, Li S, Lindgren CM, Heid IM, Berndt SI, Elliott AL, Jackson AU, Lamina
864 C, et al. 2009. Six new loci associated with body mass index highlight a neuronal influence on
865 body weight regulation. *Nat Genet* **41**: 25–34.
866 http://www.nature.com/doifinder/10.1038/ng.287.

867 Xie Y, Tang J, Xie X, Li X, Huang J, Fei Y, Han J, Chen S, Tang H, Zhao X, et al. 2019. An asymmetric
868 allelic interaction drives allele transmission bias in interspecific rice hybrids. *Nat Commun*.

869 Zajitschek SRK, Lindholm AK, Evans JP, Brooks RC. 2009. Experimental evidence that high levels of
870 inbreeding depress sperm competitiveness. *J Evol Biol* **22**: 1338–45.
871 http://doi.wiley.com/10.1111/j.1420-9101.2009.01738.x.

872 Zuk O, Hechter E, Sunyaev SR, Lander ES. 2012. The mystery of missing heritability: Genetic
873 interactions create phantom heritability. *Proc Natl Acad Sci* **109**: 1193–1198.
874 http://www.pnas.org/cgi/doi/10.1073/pnas.1119675109.

875

Supplemental files

Supplemental_Table_S1 **- *Transmission ratio distortion, allele transmissions, and p-values***

Supplemental_Table_S2 **– *Genotypes, map, and pedigree of the AIL individuals***

Supplemental_Table_S3 **- *Genes in TRD regions (All, Non-synonymous SNPs)***

Supplemental_Table_S4 **- Complete *pathway over-representation analysis***

Supplemental_File_S5 **- MAF comparison and marker density**